

Visualizing the electronic structure of kagome magnet $LuMn_6Sn_6$ by angle-resolved photoemission spectroscopy

Man Li(李满), Qi Wang(王琦), Liqin Zhou(周丽琴), Wenhua Song(宋文华), Huan Ma(马欢), Pengfei Ding(丁鹏飞), Alexander Fedorov, Yaobo Huang(黄耀波), Bernd Büchner, Hechang Lei(雷和畅), Shancai Wang(王善才), and Rui Lou(娄睿)

Citation: Chin. Phys. B, 2024, 33 (**11**): 117101. DOI: 10.1088/1674-1056/ad7afe
Journal homepage: http://cpb.iphy.ac.cn; http://iopscience.iop.org/cpb

What follows is a list of articles you may be interested in

Layered kagome compound $Na_2Ni_3S_4$ with topological flat band

Junyao Ye(叶君耀), Yihao Lin(林益浩), Haozhe Wang(王浩哲), Zhida Song(宋志达), Ji Feng(冯济), Weiwei Xie(谢韦伟), and Shuang Jia(贾爽)
Chin. Phys. B, 2024, 33 (**5**): 057103. DOI: 10.1088/1674-1056/ad3431

Band structures of strained kagome lattices

Luting Xu(徐露婷) and Fan Yang(杨帆)
Chin. Phys. B, 2024, 33 (**2**): 027101. DOI: 10.1088/1674-1056/ad0291

Flat band in hole-doped transition metal dichalcogenide observed by angle-resolved photoemission spectroscopy

Zilu Wang(王子禄), Haoyu Dong(董皓宇), Weichang Zhou(周伟昌), Zhihai Cheng(程志海), and Shancai Wang(王善才)
Chin. Phys. B, 2023, 32 (**6**): 067103. DOI: 10.1088/1674-1056/acc7f9

Robust and intrinsic type-III nodal points in a diamond-like lattice

Qing-Ya Cheng(程青亚), Yue-E Xie(谢月娥), Xiao-Hong Yan(颜晓红), and Yuan-Ping Chen(陈元平)
Chin. Phys. B, 2022, 31 (**11**): 117101. DOI: 10.1088/1674-1056/ac7c00

Intrinsic V vacancy and large magnetoresistance in $V_{1-\delta}Sb_2$ single crystal

Yong Zhang(张勇), Xinliang Huang(黄新亮), Jinglei Zhang(张警蕾), Wenshuai Gao(高文帅), Xiangde Zhu(朱相德), and Li Pi(皮雳)
Chin. Phys. B, 2022, 31 (**3**): 037102. DOI: 10.1088/1674-1056/ac3070

RAPID COMMUNICATION

Visualizing the electronic structure of kagome magnet $LuMn_6Sn_6$ by angle-resolved photoemission spectroscopy

Man Li(李满)[1,†], Qi Wang(王琦)[2], Liqin Zhou(周丽琴)[3,4], Wenhua Song(宋文华)[2], Huan Ma(马欢)[2], Pengfei Ding(丁鹏飞)[2], Alexander Fedorov[5,6,7], Yaobo Huang(黄耀波)[8], Bernd Büchner[5,9], Hechang Lei(雷和畅)[2,‡], Shancai Wang(王善才)[2,§], and Rui Lou(娄睿)[5,6,7,¶]

[1] *School of Information Network Security, People's Public Security University of China, Beijing* 100038, *China*
[2] *Department of Physics, Key Laboratory of Quantum State Construction and Manipulation (Ministry of Education), and Beijing Key Laboratory of Opto-electronic Functional Materials & Micronano Devices, Renmin University of China, Beijing* 100872, *China*
[3] *Beijing National Laboratory for Condensed Matter Physics and Institute of Physics, Chinese Academy of Sciences, Beijing* 100190, *China*
[4] *University of Chinese Academy of Sciences, Beijing* 100049, *China*
[5] *Leibniz Institute for Solid State and Materials Research, IFW Dresden, Dresden* 01069, *Germany*
[6] *Helmholtz-Zentrum Berlin für Materialien und Energie, Albert-Einstein-Straße 15, Berlin* 12489, *Germany*
[7] *Joint Laboratory "Functional Quantum Materials" at BESSY II, Berlin* 12489, *Germany*
[8] *Shanghai Advanced Research Institute, Chinese Academy of Sciences, Shanghai* 201204, *China*
[9] *Institute for Solid State and Materials Physics, TU Dresden, Dresden* 01062, *Germany*

(Received 22 July 2024; revised manuscript received 2 September 2024; accepted manuscript online 14 September 2024)

Searching for the dispersionless flat band (FB) in quantum materials, especially in topological systems, becomes an interesting topic. The kagome lattice is an ideal platform for such exploration because the FB can be naturally induced by the underlying destructive interference. Nevertheless, the magnetic kagome system that hosts the FB close to the Fermi level (E_F) is exceptionally rare. Here, we study the electronic structure of a kagome magnet $LuMn_6Sn_6$ by combining angle-resolved photoemission spectroscopy and density functional theory calculations. The observed Fermi-surface topology and overall band dispersions are similar to previous studies of the XMn_6Sn_6 (X = Dy, Tb, Gd, Y) family of compounds. We clearly observe two kagome-derived FBs extending through the entire Brillouin zone, and one of them is located just below E_F. The photon-energy-dependent measurements reveal that these FBs are nearly dispersionless along the k_z direction as well, supporting the quasi-two-dimensional character of such FBs. Our results complement the XMn_6Sn_6 family and demonstrate the robustness of the FB features across this family.

Keywords: flat band, kagome magnet, angle-resolved photoemission spectroscopy

PACS: 71.20.–b, 79.60.–i

DOI: 10.1088/1674-1056/ad7afe

1. Introduction

In recent years, there has been an increasing interest in the exploration of unique lattice geometry with novel band topologies. The most representative examples are the twisted bilayer/multilayer graphene[1–4] and kagome-structured materials. The kagome lattice, a two-dimensional (2D) honeycomb network of corner-sharing triangles, has attracted particular attention due to the presence of fertile novel properties such as charge density wave (CDW),[5–7] unconventional superconductivity,[8–10] and topological quantum states.[11–16] These exotic states have been suggested to be intimately associated with the unique electronic structure of kagome lattice, namely, the Dirac point (DP), van Hove singularities (vHSs), and flat band (FB).[17] In general, the FB can be realized in the f-electron systems, the systems with strong Coulomb interaction like Mott insulator, and the systems with unique lattice geometry like Morié lattice and kagome lattice. Regarding the FB in kagome lattice, which is derived from the destructive interference of Bloch wave functions, it can be described by Chern numbers and is interpreted as a counterpart of the Landau level without an external magnetic field. In other words, once a net magnetization and intrinsic spin–orbital coupling (SOC) are present, the well-defined topological Chern FB with nonzero Chern number, Chern gap, and even intrinsic quantum anomalous Hall effect could be realized when the Fermi energy (E_F) is tuned properly.[18–23] Meanwhile, as a highly degenerate electronic state with quenched kinetic energy, the FB may give rise to diverse exotic symmetry-breaking states, such as the high-temperature superconductivity, high-temperature ferromagnetism, Bose–Einstein condensation, and Wigner crystal.[24–29]

Recently, fruitful experimental progress has been

[†]Corresponding author. E-mail: lmrucphys@ruc.edu.cn
[‡]Corresponding author. E-mail: hlei@ruc.edu.cn
[§]Corresponding author. E-mail: scw@ruc.edu.cn
[¶]Corresponding author. E-mail: lourui09@gmail.com

© 2024 Chinese Physical Society and IOP Publishing Ltd

achieved in the realm of the kagome materials. The kagome metal AV_3Sb_5 (A = K, Rb, Cs) family has been discovered to host a variety of novel properties like the chiral CDW,[30] time-reversal symmetry breaking induced anomalous Hall effect,[31,32] rotational symmetry breaking,[33,34] pair density wave,[33] competing CDW and superconductivity,[35,36] and electronic nematicity.[37] Besides the single-layer kagome compounds AV_3Sb_5, the recently established bilayer kagome metals XR_6Sn_6 (X = Li, Sc, Y or rare-earth element; R = V, Cr, Mn), which we refer to as the 166 system, serve as another promising platform for exploring exotic correlated and topological electronic states. Rich properties have been found in the V-based 166 system, including the CDW in ScV_6Sn_6,[38–41] $\mathbb{Z}_2$ topological states in GdV_6Sn_6 and HoV_6Sn_6,[15] and anisotropic magnetism in TbV_6Sn_6.[42] However, the kagome FBs in both AV_3Sb_5 and V-based 166 systems are located away from E_F, thus contribute little to the low-energy quasiparticle excitations. This misfortune has been ended by the discovery of close-to-E_F kagome FBs in Mn-based 166 system. Despite the various magnetic ground states across the Mn-based 166 series (antiferromagnetic/ferromagnetic/ferrimagnetic), most of the compounds exhibit intrinsic anomalous Hall effect and, more importantly, host very similar overall electronic structures.[43–51] Whereas, from the perspective of transport measurements, in contrast to other Mn-based 166 materials, the antiferromagnetic $LuMn_6Sn_6$ does not show any abnormalities,[45,52] leaving its electronic properties unpredictable. Therefore, it would be interesting to explore whether the band structure of $LuMn_6Sn_6$ is different from that of other XMn_6Sn_6 compounds. Such a study can help us better understand the relationship between magnetism, electron correlations, and kagome band characteristics in the XMn_6Sn_6 family.

In this work, we systematically investigate the electronic structures of $LuMn_6Sn_6$ by ARPES measurements and density functional theory (DFT) calculations. We reveal that the overall electronic structure of $LuMn_6Sn_6$ is analogous to that of other XMn_6Sn_6 compounds. We unambiguously observe two kagome-derived FBs near E_F in $LuMn_6Sn_6$. Their negligible k_z dispersions indicate the quasi-2D character of such FB features. Our results complement the XMn_6Sn_6 family and establish an ideal magnetic kagome lattice with robust multiple FBs regardless of the underlying magnetic orders.

2. Materials and methods

The single crystals of $LuMn_6Sn_6$ were synthesized by the tin flux method. The raw materials with the molar ratio of Lu:Mn:Sn = 1:6:30 were loaded in an alumina crucible and then sealed in a quartz tube. The mixture was firstly heated to 1000 °C and maintained for 24 hours, then gradually cooled to 600 °C. The single crystals were obtained by utilizing the centrifuge to remove the excess tin flux. ARPES measurements were performed at the Dreamline beamline of the Shanghai Synchrotron Radiation Facility (SSRF) using photons with linear horizontal polarization. The optimal energy and angular resolutions were set to 15 meV and 0.1°, respectively. Samples were cleaved *in situ* along the (001) surface. During the measurements, the temperature was kept at 20 K and the pressure was maintained better than 5×10^{-11} Torr. The electron momentum parallel to the surface ($k_{\parallel}=\frac{\sqrt{2m_eK_{out}}}{\hbar}\sin\theta$) along the x and y directions can be calculated from the relation $k_x=\frac{\sqrt{2m_eK_{out}}}{\hbar}\sin\theta\cos\phi$ and $k_y=\frac{\sqrt{2m_eK_{out}}}{\hbar}\sin\theta\sin\phi$, respectively, where m_e is the mass of free electron, K_{out} is the kinetic energy of electron outside of the material, θ is the polar angle, ϕ is the azimuthal angle. The perpendicular momentum inside the material can be predicted with the relation $k_z=\sqrt{\frac{2m_e^*}{\hbar^2}(K_{out}+V_0)-\frac{2m_e}{\hbar^2}K_{out}\sin^2\phi}$ with V_0 being the empirical inner potential for the material and m_e^* being the effective mass of the electron.[53] The band structures calculations of YMn_6Sn_6/$LuMn_6Sn_6$ were performed by the Vienna *ab initio* simulation package (VASP) with the projector augmented-wave (PAW) formalism based on the DFT.[54,55] The Perdew–Burke–Ernzerhof (PBE) exchange–correlation functional with the generalized gradient approximation corrected for on-site Coulombic interactions (GGA + U) method was adopted.[56,57] The parameter U was set to be 6 eV to deal with the effect of Coulomb correction from the localized d orbitals of Y/Lu atoms. The cutoff energy for the plane-wave basis was set to be 500 eV and a $9\times9\times5$-centered mesh was implemented for the Brillouin zone (BZ) integral sampling. The local magnetic moments of Mn atoms were along the z axis. The SOC effect was taken into account in all calculations.

3. Results and discussion

As illustrated in Fig. 1(a), $LuMn_6Sn_6$ crystallizes in a hexagonal structure with the space group $P6/mmm$ (No. 191), consisting of an alternative stacking of $LuSn_2$, Mn_3Sn, and Sn layers along the c axis. The Lu-based triangular and Mn-based kagome sublattices are clearly visualized in a top view of the $LuMn_6Sn_6$ structure in Fig. 1(b). The bulk and (001)-projected surface BZs of $LuMn_6Sn_6$ are depicted in Fig. 1(c). The tight-binding electronic structure of a 2D kagome lattice is characterized by the coexistence of DP at the BZ corner, vHSs at the BZ boundary, and FB over the whole BZ, as illustrated in Fig. 1(d). In Fig. 1(e), we present the Fermi surface mapping of $LuMn_6Sn_6$ taken at $k_z\sim0$ plane. The Fermi surface consists of the warped electron pocket around the Γ point and the triangular features at the K point, both with strong matrix element effect modulating the intensities in different BZs.[58] The Fermi surface topology of $LuMn_6Sn_6$ is in analogy to that of other XMn_6Sn_6 kagome compounds, implying

that their band structure might be similar. The core-level photoemission spectrum in Fig. 1(f) shows the characteristic peaks of Lu-5p/4f, Mn-3p, and Sn-4d orbitals, further confirming the elemental composition of the $LuMn_6Sn_6$ sample. At low temperatures, the magnetic moments of the Mn atoms align ferromagnetically within each kagome layer; the moments of adjacent kagome layers couple antiferromagnetically and ferromagnetically across the non-magnetic $LuSn_2$ and Sn layers, respectively, resulting in the formation of the incommensurate helical antiferromagnetism, which is similar but still a bit different compared to that in YMn_6Sn_6.[52] The detailed magnetic properties of $LuMn_6Sn_6$ are yet to be confirmed by the neutron scattering experiments in the future.

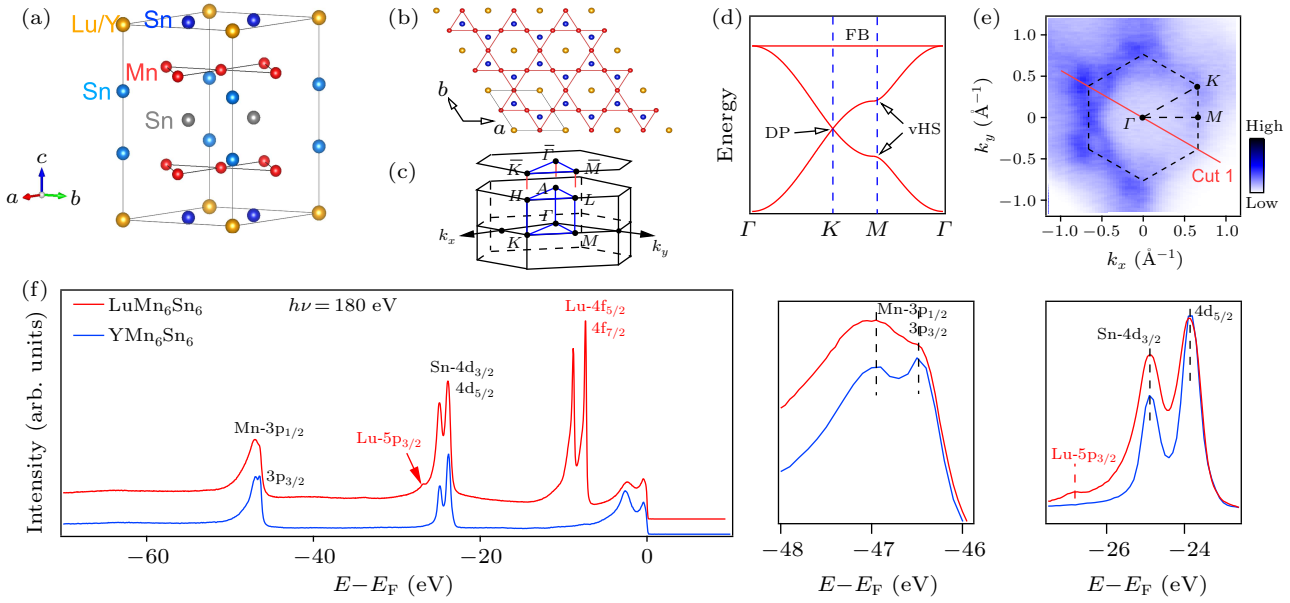


Fig. 1. Crystal structure and electronic structure of $LuMn_6Sn_6$. (a) Schematic crystal structure of Lu(Y)Mn_6Sn_6 with space group $P6/mmm$ (No. 191). (b) Top view of the Lu(Y)Mn_6Sn_6 crystal structure. (c) Bulk and (001)-projected surface BZs. (d) Tight-binding band structure calculation of a kagome lattice showing the DP, vHSs, and FB. (e) ARPES intensity plot measured with 138-eV photons at $E_F \pm 10$ meV in the $k_z \sim 0$ plane. (f) Core-level photoemission spectra of $LuMn_6Sn_6$ and YMn_6Sn_6 recorded at $h\nu = 180$ eV. The characteristic peaks of the elements are marked out.

The electronic band dispersions of $LuMn_6Sn_6$ are summarized in Fig. 2, where we also plot the results of YMn_6Sn_6 for comparison. Figures 2(a) and 2(b) show their ARPES intensities and corresponding second derivative intensities along the Γ–K–M–K–Γ' directions [indicated by cut 1 in Fig. 1(e)]. We notice that $LuMn_6Sn_6$ shares quite analogous overall band structure with YMn_6Sn_6, as well as with other $X Mn_6Sn_6$ compounds.[46,48,50,51] Along the Γ–K–M–K–Γ' direction, one can clearly see a parabolic electron-like band around the Γ point and a FB (denoted as FB2) at about -0.4 eV. The FB2 appears to show discontinuity when crossing the parabolic band, indicating the potential SOC gap opening, similar to the case of other kagome prototype materials.[50,51,59,60] Moreover, one observes a dispersionless feature near E_F (at about -0.1 eV) that is faint in the 1st BZ but more intense in the extended BZ, this is another kagome-derived FB (denoted as FB1). We attribute this contrasting behavior of the FB1 to the BZ selection effects, i.e., the matrix element effects, which manifest as different photoemission intensities between the first BZ and the extended BZ.[58] Such observation is also consistent with the previous studies of other $X Mn_6Sn_6$ compounds.[48,51] It is noted that, due to the simultaneous presence of multiple band dispersions near E_F, the FB1 appears to be dispersive and broad in energy. Meanwhile, as guided by the red solid curves in the second derivative intensity plots, a DP is formed at the K point just below E_F. These typical kagome band features (FB1, FB2, and DP) of $LuMn_6Sn_6$ and YMn_6Sn_6 have also been identified at similar energy scales in other $X Mn_6Sn_6$ compounds.[48,50,51] The flat bands (FB1 and FB2), parabolic electron-like band, and Dirac-like band (DP) can be further visualized from the energy distribution curves (EDCs), as displayed in Fig. 2(c).

Our observations of the parabolic electron-like band, DP, and FB2 can be well captured by the bulk DFT calculations shown in Figs. 2(d) and 2(e). For the electronic band structure near the E_F, which is constructed by Mn-3d electronic systems, it is essential to account for correlation effects. A moderate band renormalization factor of about 1.7 and 1.63 has to be used to compare the calculated and observed band structures in YMn_6Sn_6 and $LuMn_6Sn_6$, respectively. However, the FB1 in the vicinity of E_F has not been reproduced by the present calculations. It is interesting to note that the FB1 is actually not well described by the DFT calculations in all $X Mn_6Sn_6$ compounds.[46–48,50] This discrepancy can be perfectly resolved by performing DFT plus dynamical mean-field theory (DMFT) calculations, which provide a better treatment of the

many-body correlation effects. Such fact has been proved by our previous DFT + DMFT calculations of YMn_6Sn_6.[51] As a result, we infer that the double FB structure in XMn_6Sn_6 is derived from the ferromagnetic exchange splitting in the Mn-based kagome plane. To quantify the energy scale of such band splitting, we display the momentum-integrated (along K–Γ' line) energy distribution curves in the insets of Figs. 2(a) and 2(b). The energy separation between FB1 and FB2 is about 0.3 eV for both $LuMn_6Sn_6$ and YMn_6Sn_6, comparable with that of other XMn_6Sn_6 compounds.[48] On the other hand, in the Mn-166 system, the near-E_F vHS1 has been revealed at the M point, which has the similar energy position as the FB1.[48,51,61] Similarly, the FB2 and vHS2 at Γ point also share a similar energy level. The high density of states contributed by the vHSs can potentially give rise to emergent correlated states. Nonetheless, since both the FB1 and FB2 are extended over the entire BZ in experiments, the possibility that they arise from the enhanced electron scattering near the vHSs can be ruled out.

Then we carry out the k_z-dependent measurements by varying the incident photon energy from 76 eV to 172 eV, which covers more than two BZs along the k_z direction. The lower panel of Fig. 3(a) shows the three-dimensional intensity plot of the electronic structure of $LuMn_6Sn_6$ for the $h\nu$–$k_{\|}$ plane, with the $k_{\|}$ oriented along the $\bar{\Gamma}$–$\bar{K}$ direction, as indicated by the orange shaded area in the upper panel of Fig. 3(a). The FB1 close to E_F is clearly observed in the 3rd BZ. It is nearly dispersionless with the bandwidth smaller than 0.1 eV as changing the photon energy, indicating its quasi-2D character. Similarly, the FB2 at about 0.37 eV below E_F is clearly revealed across the studied photon energy interval. It also exhibits the quasi-2D nature with a bandwidth smaller than 0.15 eV. In Fig. 3(b), we display the detailed band dispersions along the $\bar{\Gamma}$–$\bar{K}$–$\bar{M}$–K–$\bar{\Gamma}'$ lines under different photon energies (120 eV, 130 eV, 140 eV, 150 eV, 160 eV, and 170 eV). One can unambiguously see the FB1 near E_F around the 3rd BZ center and the FB2 at higher binding energy over a wide momentum range. Consistently, there are no noticeable variations of their energy positions, as illustrated in the k_z mapping data in Fig. 3(a).

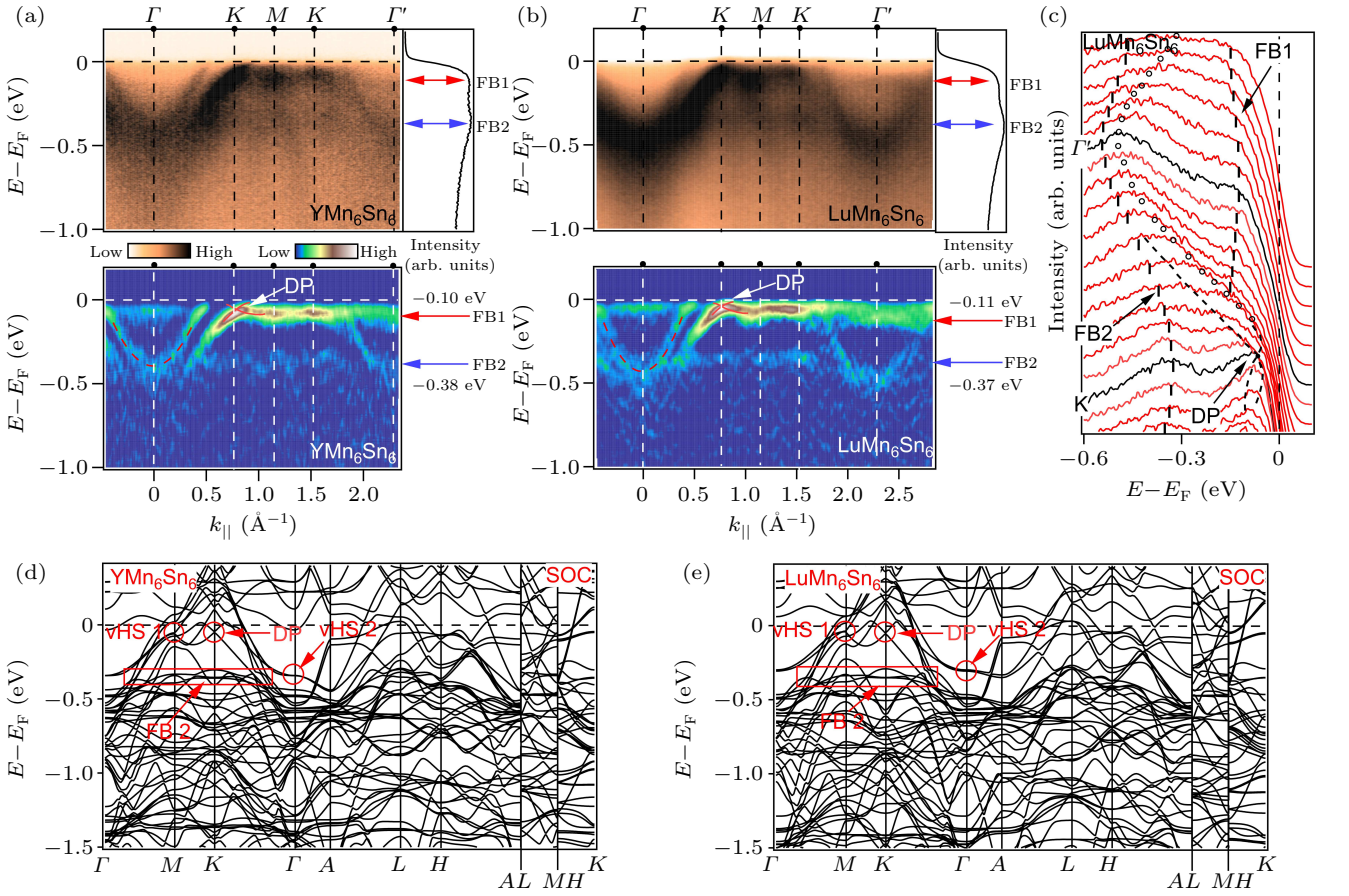


Fig. 2. Key signatures of kagome band structure. (a) and (b) Photoemission intensity plots and corresponding second derivative plots of YMn_6Sn_6 and $LuMn_6Sn_6$ along high-symmetry line taken with 138-eV photons ($k_z \sim 0$ plane), respectively, with the momentum path indicated in Fig. 1(e) (cut 1). The momentum-integrated energy distribution curve (integrated over K–Γ') is overlaid, with a double-headed arrow indicating the FB peaks. The parabolic band around Γ point and the Dirac-cone (DP) at K point are indicated by the red dashed curve and red solid curves, respectively. (c) EDC plots of (b) over the momentum range of $1.3 < k_{\|} < 2.8$. The flat bands (FB1 and FB2) and the Dirac-cone (DP) are indicated by the thick and thin black dashed lines, respectively. The parabolic electron-like band is indicated by open circles. (d) and (e) Calculated band structures of YMn_6Sn_6 and $LuMn_6Sn_6$ with the SOC effect along high-symmetry lines, renormalized by factors of about 1.7 and 1.63, respectively.

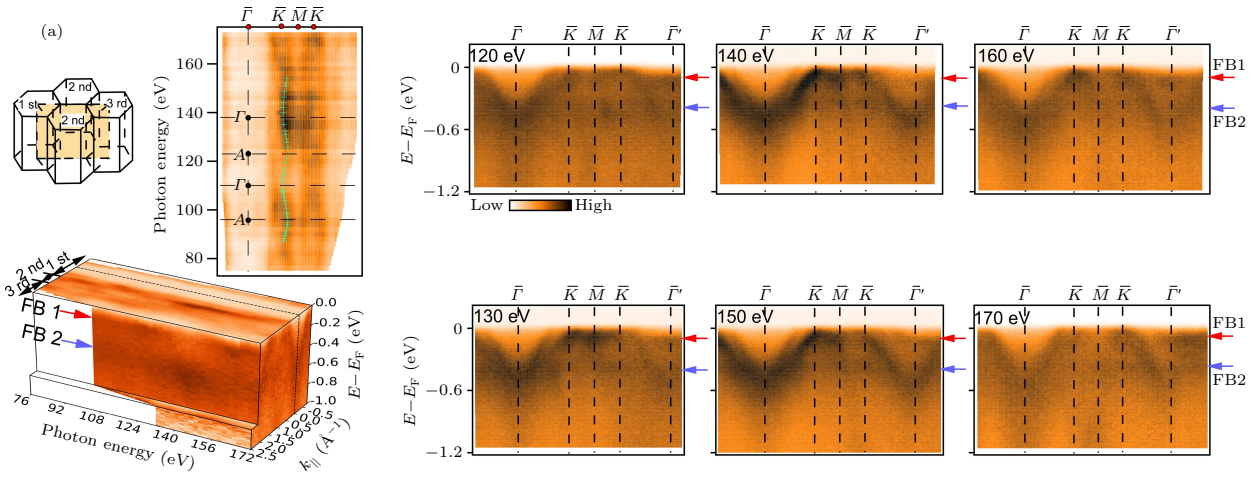


Fig. 3. Photon-energy-dependent measurements of $LuMn_6Sn_6$. (a) Fermi surface and three-dimensional intensity plot of the electronic structure of $LuMn_6Sn_6$ for the $h\nu$–$k_{\parallel}$ plane, with the $k_{\parallel}$ oriented along the $\bar{\Gamma}$–$\bar{K}$ direction. The corresponding momentum location is indicated by the orange shaded area in the upper left panel. The green markers are guides to the eye for the measured k_z dispersion. (b) ARPES intensity plots measured at different photon energies. The red and blue arrows indicate the locations of FBs.

The previous studies indicate that the YMn_6Sn_6 and $LuMn_6Sn_6$ have an incommensurate helical antiferromagnetic structure with some differences.[52] Experimental investigations into the magnetic properties of YMn_6Sn_6 have been conducted,[62] whereas the magnetic configuration of $LuMn_6Sn_6$ is yet to be unveiled. Although our results undoubtedly reveal similar electronic structures of YMn_6Sn_6 and $LuMn_6Sn_6$, they manifest distinct characteristics in the transport measurements, in particular, the intrinsic anomalous Hall conductivity is large in the former while is vanishingly weak in the latter.[63] Such phenomena in these two compounds lack a satisfactory explanation at present, as well as for the other XMn_6Sn_6 materials. It has been suggested that the giant intrinsic anomalous Hall effect in kagome lattice is intimately related to the large Berry curvature of the massive Dirac fermions, whose gap/mass is dominated by the Kane–Mele type SOC effect. Such SOC has been found to be sensitive to the fine structure of the magnetic configurations, like the orientation and canting angle of the moments, as observed in Fe_3Sn_2[64] and Fe_3Ge.[65] Therefore, based on our results, we infer that the distinct transport properties of YMn_6Sn_6 and $LuMn_6Sn_6$ as well as other XMn_6Sn_6 compounds can be attributed to their subtle differences in the SOC gap size, which are most likely derived from their differing magnetic configurations.

Last, we briefly compare the properties of Mn-166 system and Cr-166 system, which serves as a bridge between the V-166 and Mn-166 families. Recent experimental studies of YCr_6Ge_6[66] and $CsCr_6Sb_6$[67] compounds show that the FB is located even closer to the Fermi level compared to Mn-166 system, providing an excellent platform for further engineering the FB through doping, electrical gating, or dimensional reduction. Therefore, it is reasonable to expect that the Cr-doped Mn-166 kagome materials could be an appealing playground for exploring the novel quantum phenomena associated with the correlation effects of FB, such as the unconventional superconductivity and quantum anomalous Hall effect.

4. Conclusion and outlook

In summary, we have studied the electronic structure of the kagome magnet $LuMn_6Sn_6$ by ARPES experiments and DFT calculations. We find that there are two kagome-derived FBs near E_F, which remain nearly dispersionless also along the k_z direction. By comparing the electronic structures of $LuMn_6Sn_6$ and YMn_6Sn_6, we substantiate that the near-E_F band structure of XMn_6Sn_6 family is similar and robust, regardless of the various magnetic properties within this family. Since one of the FBs is located just below E_F, the effect of different carrier doping levels introduced by the X elements is inconspicuous. As a result, the energy positions of the FBs as well as other main band features are almost the same across the XMn_6Sn_6 family. Our results suggest the XMn_6Sn_6 family as a robust and ideal platform to investigate and engineer the FB-related physics.

Acknowledgments

Project supported by the National Natural Science Foundation of China (Grant No. 12204536), the Fundamental Research Funds for the Central Universities, and the Research Funds of People's Public Security University of China (PPSUC) (Grant No. 2023JKF02ZK09).

References

[1] Chen S, He M, Zhang Y H, Hsieh V, Fei Z, Watanabe K, Taniguchi T, Cobden D H, Xu X, Dean C R and Yankowitz M 2021 *Nat. Phys.* **17** 374
[2] Cao Y, Fatemi V, Fang S, Watanabe K, Taniguchi T, Kaxiras E and Jarillo-Herrero P 2018 *Nature* **556** 43
[3] Lisi S, Lu X, Benschop T, *et al.* 2021 *Nat. Phys.* **17** 189
[4] Han T, Lu Z, Scuri G, Sung J, Wang J, Han T, Watanabe K, Taniguchi T, Park H and Ju L 2024 *Nat. Nanotechnol.* **19** 181

[5] Neupert T, Denner M M, Yin J X, Thomale R and Hasan M Z 2022 *Nat. Phys.* **18** 137

[6] Teng X, Chen L, Ye F, Rosenberg E, Liu Z, Yin J X, Jiang Y X, Oh J S, Hasan M Z, Neubauer K J, Gao B, Xie Y, Hashimoto M, Lu D, Jozwiak C, Bostwick A, Rotenberg E, Birgeneau R J, Chu J H, Yi M and Dai P 2022 *Nature* **609** 490

[7] Lou R, Fedorov A, Yin Q, Kuibarov A, Tu Z, Gong C, Schwier E F, Büchner B, Lei H and Borisenko S 2022 *Phys. Rev. Lett.* **128** 036402

[8] Ko W H, Lee P A and Wen X G 2009 *Phys. Rev. B* **79** 214502

[9] Kiesel M L, Platt C and Thomale R 2013 *Phys. Rev. Lett.* **110** 126405

[10] Zhong Y, Liu J, Wu X, *et al.* 2023 *Nature* **617** 488

[11] Xu G, Lian B and Zhang S C 2015 *Phys. Rev. Lett.* **115** 186802

[12] Yin J X, Ma W, Cochran T A, *et al.* 2020 *Nature* **583** 533

[13] Zhang T, Yilmaz T, Vescovo E, Li H X, Moore R G, Lee H N, Miao H, Murakami S and McGuire M A 2022 *npj Comput. Mater.* **8** 155

[14] Wang Y, Wu H, McCandless G T, Chan J Y and Ali M N 2023 *Nat. Rev. Phys.* **5** 635

[15] Peng S, Han Y, Pokharel G, Shen J, Li Z, Hashimoto M, Lu D, Ortiz B R, Luo Y, Li H, Guo M, Wang B, Cui S, Sun Z, Qiao Z, Wilson S D and He J 2021 *Phys. Rev. Lett.* **127** 266401

[16] Yin J X, Lian B and Hasan M Z 2022 *Nature* **612** 647

[17] Liu Z, Liu F and Wu Y S 2014 *Chin. Phys. B* **23** 077308

[18] Ohgushi K, Murakami S and Nagaosa N 2000 *Phys. Rev. B* **62** R6065

[19] Sun K, Gu Z, Katsura H and Das Sarma S 2011 *Phys. Rev. Lett.* **106** 236803

[20] Venderbos J W F, Daghofer M and van den Brink J 2011 *Phys. Rev. Lett.* **107** 116401

[21] Neupert T, Santos L, Chamon C and Mudry C 2011 *Phys. Rev. Lett.* **106** 236804

[22] Tang E, Mei J W and Wen X G 2011 *Phys. Rev. Lett.* **106** 236802

[23] Liu Z, Wang Z F, Mei J W, Wu Y S and Liu F 2013 *Phys. Rev. Lett.* **110** 106804

[24] Mielke A 1991 *J. Phys. A: Math. General* **24** 3311

[25] Mielke A 1992 *J. Phys. A: Math. General* **25** 4335

[26] Imada M and Kohno M 2000 *Phys. Rev. Lett.* **84** 143

[27] Peotta S and Törmä P 2015 *Nat. Commun.* **6** 8944

[28] Huber S D and Altman E 2010 *Phys. Rev. B* **82** 184502

[29] Wu C, Bergman D, Balents L and Das Sarma S 2007 *Phys. Rev. Lett.* **99** 070401

[30] Jiang Y X, Yin J X, Denner M M, *et al.* 2021 *Nat. Mater.* **20** 1353

[31] Yang S Y, Wang Y, Ortiz B R, Liu D, Gayles J, Derunova E, Gonzalez-Hernandez R, Šmejkal L, Chen Y, Parkin S S P, Wilson S D, Toberer E S, McQueen T and Ali M N 2020 *Sci. Adv.* **6** eabb6003

[32] Mielke C, Das D, Yin J X, *et al.* 2022 *Nature* **602** 245

[33] Zhao H, Li H, Ortiz B R, Teicher S M L, Park T, Ye M, Wang Z, Balents L, Wilson S D and Zeljkovic I 2021 *Nature* **599** 216

[34] Chen H, Yang H, Hu B, Zhao Z, Yuan J, Xing Y, Qian G, Huang Z, Li G, Ye Y, Ma S, Ni S, Zhang H, Yin Q, Gong C, Tu Z, Lei H, Tan H, Zhou S, Shen C, Dong X, Yan B, Wang Z and Gao H J 2021 *Nature* **599** 222

[35] Chen K Y, Wang N N, Yin Q W, Gu Y H, Jiang K, Tu Z J, Gong C S, Uwatoko Y, Sun J P, Lei H C, Hu J P and Cheng J G 2021 *Phys. Rev. Lett.* **126** 247001

[36] Yu F H, Ma D H, Zhuo W Z, Liu S Q, Wen X K, Lei B, Ying J J and Chen X H 2021 *Nat. Commun.* **12** 3645

[37] Nie L, Sun K, Ma W, Song D, Zheng L, Liang Z, Wu P, Yu F, Li J, Shan M, Zhao D, Li S, Kang B, Wu Z, Zhou Y, Liu K, Xiang Z, Ying J, Wang Z, Wu T and Chen X 2022 *Nature* **604** 59

[38] Arachchige H W S, Meier W R, Marshall M, Matsuoka T, Xue R, McGuire M A, Hermann R P, Cao H and Mandrus D 2022 *Phys. Rev. Lett.* **129** 216402

[39] Hu T, Pi H, Xu S, Yue L, Wu Q, Liu Q, Zhang S, Li R, Zhou X, Yuan J, Wu D, Dong T, Weng H and Wang N 2023 *Phys. Rev. B* **107** 165119

[40] Hu Y, Ma J, Li Y, Gawryluk D J, Hu T, Teyssier J, Multian V, Yin Z, Jiang Y, Xu S, Shin S, Plokhikh I, Han X, Plumb N C, Liu Y, Yin J, Guguchia Z, Zhao Y, Schnyder A P, Wu X, Pomjakushina E, Hasan M Z, Wang N and Shi M 2023 2024 *Nat. Commun.* **15** 1658

[41] Korshunov A, Hu H, Subires D, Jiang Y, Călugăru D, Feng X, Rajapitamahuni A, Yi C, Roychowdhury S, Vergniory M G, Strempfer J, Shekhar C, Vescovo E, Chernyshov D, Said A H, Bosak A, Felser C, Bernevig B A and Blanco-Canosa S 2023 *Nat. Commun.* **14** 6646

[42] Pokharel G, Ortiz B, Chamorro J, Sarte P, Kautzsch L, Wu G, Ruff J and Wilson S D 2022 *Phys. Rev. Mater.* **6** 104202

[43] Haldane F D M 2004 *Phys. Rev. Lett.* **93** 206602

[44] Ma W, Xu X, Wang Z, Zhou H, Marshall M, Qu Z, Xie W and Jia S 2021 *Phys. Rev. B* **103** 235109

[45] Ma W, Xu X, Yin J X, Yang H, Zhou H, Cheng Z J, Huang Y, Qu Z, Wang F, Hasan M Z and Jia S 2021 *Phys. Rev. Lett.* **126** 246602

[46] Dhakal G, Cheenicode Kabeer F, Pathak A K, Kabir F, Poudel N, Filippone R, Casey J, Pradhan Sakhya A, Regmi S, Sims C, Dimitri K, Manfrinetti P, Gofryk K, Oppeneer P M and Neupane M 2021 *Phys. Rev. B* **104** L161115

[47] Chen D, Le C, Fu C, Lin H, Schnelle W, Sun Y and Felser C 2021 *Phys. Rev. B* **103** 144410

[48] Gu X, Chen C, Wei W S, *et al.* 2022 *Phys. Rev. B* **105** 155108

[49] Wang Q, Neubauer K J, Duan C, Yin Q, Fujitsu S, Hosono H, Ye F, Zhang R, Chi S, Krycka K, Lei H and Dai P 2021 *Phys. Rev. B* **103** 014416

[50] Liu Z, Zhao N, Li M, Yin Q, Wang Q, Liu Z, Shen D, Huang Y, Lei H, Liu K and Wang S 2021 *Phys. Rev. B* **104** 115122

[51] Li M, Wang Q, Wang G, Yuan Z, Song W, Lou R, Liu Z, Huang Y, Liu Z, Lei H, Yin Z and Wang S 2021 *Nat. Commun.* **12** 3129

[52] Venturini G, Fruchart D and Malaman B 1996 *J. Alloys Compd.* **236** 102

[53] Hüfner S 2003 *Photoelectron Spectroscopy: Principles and Applications* (Berlin: Springer)

[54] Kresse G and Furthmüller J 1996 *Phys. Rev. B* **54** 11169

[55] Kresse G and Joubert D 1999 *Phys. Rev. B* **59** 1758

[56] Perdew J P, Burke K and Ernzerhof M 1996 *Phys. Rev. Lett.* **77** 3865

[57] Kulik H J, Cococcioni M, Scherlis D A and Marzari N 2006 *Phys. Rev. Lett.* **97** 103001

[58] Shirley E L, Terminello L J, Santoni A and Himpsel F J 1995 *Phys. Rev. B* **51** 13614

[59] Kang M, Fang S, Ye L, Po H C, Denlinger J, Jozwiak C, Bostwick A, Rotenberg E, Kaxiras E, Checkelsky J G and Comin R 2020 *Nat. Commun.* **11** 4004

[60] Liu Z, Li M, Wang Q, Wang G, Wen C, Jiang K, Lu X, Yan S, Huang Y, Shen D, Yin J X, Wang Z, Yin Z, Lei H and Wang S 2020 *Nat. Commun.* **11** 4002

[61] Li H, Zhao H, Jiang K, Wang Q, Yin Q, Zhao N N, Liu K, Wang Z, Lei H and Zeljkovic I 2022 *Nat. Phys.* **18** 644

[62] Ghimire N J, Dally R L, Poudel L, Jones D C, Michel D, Magar N T, Bleuel M, McGuire M A, Jiang J S, Mitchell J F, Lynn J W and Mazin I I 2020 *Sci. Adv.* **6** eabe2680

[63] Li L, Chi S, Ma W, Guo K, Xu G and Jia S 2024 *Chin. Phys. B* **33** 057501

[64] Yin J X, Zhang S S, Li H, *et al.* 2018 *Nature* **562** 91

[65] Lou R, Zhou L, Song W, Fedorov A, Tu Z, Jiang B, Wang Q, Li M, Liu Z, Chen X, Rader O, Büchner B, Sun Y, Weng H, Lei H and Wang S 2023 arXiv: 2309.06399 [cond-mat.str-el]

[66] Yang T Y, Wan Q, Song J P, Du Z, Tang J, Wang Z W, Plumb N C, Radovic M, Wang G W, Wang G Y, Sun Z, Yin J X, Chen Z H, Huang Y B, Yu R, Shi M, Xiong Y M and Xu N 2022 *Quantum Frontiers* **1** 14

[67] Song B, Xie Y, Li W J, Liu H, Zhang Q, gang Guo J, Zhao L, Yu S L, Zhou X, Chen X and Ying T 2024 arXiv:2404.12374 [cond-mat.str-el]